

Binary Tomography Reconstruction From Few Projections With Level-set Regularization Methods For Bone Microstructure Study

L.Wang¹, B.Sixou¹, S.Rit¹, F.Peyrin^{1,2}

¹CREATIS, CNRS UMR 5220, Inserm U1044, INSA de Lyon, Universite de Lyon, F-69621, bruno.sxiou@insa-lyon.fr

²ESRF, 6 rue Jules Horowitz, F-38043, Grenoble Cedex France, peyrin@esrf.fr

ABSTRACT

Discrete tomography refers to a class of reconstruction methods adapted to discrete-valued images. A number of methods have specifically been developed to address the binary case, when a two-phase object is considered. This problem may arise in different medical applications such as vascular or bone imaging where the goal is to reduce the number of projections. In this paper, we address the problem of binary image reconstruction for X-ray CT imaging from a small number of projections. We propose two new schemes based on level-set regularization. In the first approach, the binary tomography problem is formulated as a nonlinear inverse problem and regularized with Bounded Variation-Sobolev terms. A second level-set type method is investigated which includes the binary constraints in an augmented Lagrangian. For comparison, we consider a classical TV regularization method. The three schemes are applied to a simple disk image and to bone cross-sections images of various size without and with an additive Gaussian noise. The best binary reconstruction results are obtained with the TV algorithm for the simple disk image. Lower reconstruction errors are achieved with the level-set approaches methods for a more complex bone geometry and for the higher noise levels.

Keywords: X-ray imaging, discrete tomography, level-set regularization, inverse problems.

Mathematics Subject Classification: 65J20, 65J22, 65K10, 65R10.

1 Introduction

Tomography reconstruction from a limited number of projections is an important problem in X-ray CT. It is particularly crucial when imaging a moving organ, such as the beating heart or when the irradiation dose has to be reduced. Several reconstruction methods have been proposed to achieve low dose CT. These methods are generally iterative and rely on the use of specific priors on the imaged object. Recently, with the development of compressive sensing approaches, a number of algorithms based on TV regularization schemes have been proposed (Sidky and Pan, 2008; Sidky and Pan, 2006; Ritschl, Bergner, Fleischmann and Kachelriess, 2011). These methods rely on a sparsity prior that may be applied in the image domain or after applying a sparsifying transform such as a wavelet transform. A key issue in this problem

is to improve spatial resolution without increasing irradiation dose. To this aim, it is interesting to study the potential of new optimization schemes to reconstruct images from a limited number of projections. Other approaches are based on discrete tomography making the assumption that the image is a discrete valued function (Herman and Kuba, 2007). A number of methods have specifically been developed to address the binary case, when a two-phase object is considered. The binary tomography problem is associated with an under-determined linear system of equations with the linear Radon projection operator R and binary constraints:

$$Rf = p^\delta \quad f = (f_1, \dots, f_n) \in \{0, 1\}^n \quad (1.1)$$

relating the pixel values $(f_i)_{1 \leq i \leq n}$ of the image and the measured projection value p^δ which is some approximation of the correct data p , corresponding to the true solution f^* with $Rf^* = p$. The noisy data p^δ is corrupted by noise with a noise level δ , satisfying $\|p^\delta - p\|_2 \leq \delta$.

Various approaches have been proposed to solve this reconstruction problem often based on discrete algebraic reconstruction techniques (Batenburg and Sijbers, 2009; Cai and Ma, 2010). Some methods minimize a functional that incorporates a data term and a binary constraint, with stochastic techniques (Rusko and Kuba, 2005) or convex analysis optimization (Capricelli and Combettes, 2007; Schlea, Schnrre, Webera and Horneggerb, 2005). Markov random fields have also been much used (Liao and Herman, 2004). Recently, a Belief Propagation reconstruction approach has been proposed (Gouillart, Krzakala, Mezard and Zdeborov, 2013). The binary tomography problem is ill-posed and must be regularized. The Total Variation regularization has often been used and this method gives good results (Gouillart et al., 2013). On the other hand, level-set methods, well established in the field of image processing, have been designed recently to reconstruct solutions of inverse problems with non-smooth and piecewise constant solutions (Egger and Leitao, 2009; DeCezaro, Leitao and Tai, 2009; Tai and Chan, 2004; DeCezaro, Leitao and Tai, 2013). These methods improve the classical Tikhonov regularization which gives poor results for the reconstruction of non-smooth solutions. They can be extended to the general discrete case in which the image to be reconstructed can take several discrete values. Yet, the level-set methods have never been applied to the binary tomography problem.

The main contribution of this work is to use the level-set regularization methods for the discrete parallel tomography problem and to make an extensive comparison with the TV regularization method. In this case, the direct operator is the Radon projector. We start from a formulation of the discrete tomography problem as a nonlinear inverse problem with specific constraints on the function to be reconstructed. A level-set scheme with $H_1 - BV$ regularization (DeCezaro et al., 2009) and a Piecewise Constant Level-set approach with an augmented Lagrangian approach are used to solve this nonlinear problem (DeCezaro et al., 2013). Then we compare the results and the reconstruction errors obtained with this new methods and with the classical TV regularization functional minimized by the Alternate Direction of Minimization Method (ADMM) algorithm. The comparison of the inversion schemes is performed on a simple disk and on a more complex bone CT cross-section characterized by large homogeneous regions but also elongated and tubular structures.

This paper is structured as follows. After the introduction, the second section of this paper deals with the Total Variation regularization method and the ADMM minimization methodology.

Then, the nonlinear inverse problem formulation of the binary tomography problem is presented together with the level-set regularization. The next section describes the piecewise constant level-set method and the Lagrangian approach. The numerical results obtained on a simple disk or on noisy bone CT cross-sections of various size are reported and discussed in the last section. We then give the main conclusions and perspectives of our work.

2 Total Variation regularization and ADMM approach

A common way to regularize the binary tomography problem is to construct a regularization functional $E(f)$ with a data fidelity term that measures the consistency between the estimates and the measurements and a regularization term $J(f)$ that imposes an a priori constraint on the solution. The data-fitting term is usually based on the L_2 norm and the regularization functional can then be written as:

$$E(f) = \frac{\mu}{2} \left\| Rf - p^\delta \right\|_{L_2}^2 + J(f) \quad (2.1)$$

The parameter μ is the regularization parameter balancing the contribution of the two terms. In the classical Tikhonov regularization, the regularization term is given by $J(f) = \|Df\|_2^2$, where D is a differential operator. The Total Variation regularization was introduced by Rudin et al. (Rudin, Osher and Fatemi, 2013) to solve the noise removal problem. It has been applied to various image processing problems (Ng, Weiss and Yuan, 2010) and it is very successful to preserve edges but it tends to minimize the perimeter of the distinct regions inside the image. Let Ω be a bounded open subset of \mathbb{R}^2 , for an image $f \in H_1(\Omega)$, this regularization is based on computing the L_1 norm of the gradient:

$$J_{TV}(f) = \int_{\Omega} |\nabla f(r)| dr \quad (2.2)$$

Some convex constraints can be included in the regularization functional (Afonso, Bioucas-Dias and Figueiredo, 2011; Afonso, Bioucas-Dias and Figueiredo, 2010). In this work, we restrict to a simple TV regularization without additional constraints. For comparison with the level-set regularization results presented in the next section, we have tried to solve the discrete reconstruction tomography problem with the Total Variation regularization. The following optimization problem (P) has been considered:

$$(P) \quad \text{minimize} \quad \frac{\mu}{2} \|p^\delta - Rf\|_2^2 + J_{TV}(f) \quad (2.3)$$

Various numerical methods have been used to solve the TV regularized deconvolution problem including partial differential equations or primal dual methods (Becker, Bobin and Candes, 2009). Results of extensive numerical experiments show that algorithms based on the Alternate Direction of Minimization Method (ADMM) are among the state-of-the-art methods (Afonso et al., 2011; Afonso et al., 2010; Ng et al., 2010). Algorithms based on the alternate direction of minimization (SALSA and C-SALSA) (Afonso et al., 2011; Afonso et al., 2010) have also been proposed to solve a number of image processing tasks, such as image painting and

deblurring. Our problem is thus formulated as a minimization problem of the ADMM form with linear constraints. The following augmented Lagrangian is considered:

$$\mathcal{L}(f, (g_i), (\lambda_i)) = \sum_i (\|g_i\|_2 - \lambda_i^t (g_i - D_i f) + \frac{\beta}{2} \|g_i - D_i f\|_2^2) + \frac{\mu}{2} \|p^\delta - Rf\|_2^2 \quad (2.4)$$

where μ is the regularization parameter, β the Lagrangian parameter. The Lagrange multipliers $(\lambda_i)_{1 \leq i \leq n}$, is a vector in \mathbb{R}^{2n^2} . For each pixel i , $D_i f \in \mathbb{R}^2$ represents the first-order finite difference at pixel i in both horizontal and vertical directions, $(g_i)_{1 \leq i \leq n}$ is the auxiliary unknown corresponding to the gradient. The ADMM algorithm searches for the saddle point of the augmented Lagrangian by iterating the following equations:

$$g_i^{k+1} = \arg \min_{g_i} \mathcal{L}(f^k, (g_i^k), (\lambda_i^k)) \quad (2.5)$$

$$f^{k+1} = \arg \min_f \mathcal{L}(f, (g_i^{k+1}), (\lambda_i^k)) \quad (2.6)$$

$$\lambda_i^{k+1} = \arg \min_{\lambda_i} \mathcal{L}(f^{k+1}, (g_i^{k+1}), (\lambda_i^k)) \quad (2.7)$$

In this work, we have used the isotropic TV and the l_2 norm of the gradient. With the alternating minimization algorithm, the sequences $(f^k, (g_i^k)_{1 \leq i \leq n}, (\lambda_i^k)_{1 \leq i \leq n})$ are constructed with the following iterative scheme:

$$g_i^{k+1} = \max\{\|D_i f^k + \frac{1}{\beta}(\lambda_i^k)\| - \frac{1}{\beta}, 0\} \frac{D_i f^k + \frac{1}{\beta}(\lambda_i^k)}{\|D_i f^k + \frac{1}{\beta}(\lambda_i^k)\|} \quad (2.8)$$

The new iterate f^{k+1} is obtained from the following linear system:

$$\left(\sum_i D_i^t D_i + \frac{\mu}{\beta} R^t R\right) f^{k+1} = \sum_i D_i^t (g_i^{k+1} - \frac{1}{\beta} \lambda_i^k) + \frac{\mu}{\beta} R^t p^\delta \quad (2.9)$$

The Lagrange multipliers (λ_i) are updated with:

$$\lambda_i^{k+1} = \lambda_i^k - \beta(g_i^{k+1} - D_i f^{k+1}) \quad (2.10)$$

The sequence $(f^k, (g_i^k), (\lambda_i^k))$ which is generated by the ADMM algorithm converges to a Kuhn-Tucker point of problem (P), $(f^*, (g_i^*), (\lambda_i^*))$, if (P) has one. If (P) does not have an optimal solution, then at least one of the sequences diverges.

3 Level-set regularization of the binary tomography inverse problem

3.1 Nonlinear inverse problem formulation of the binary tomography problem

Our new level-set treatment of the binary tomography is based on a reformulation of the reconstruction as a nonlinear inverse problem and on representation of the function to be reconstructed with a Heaviside distribution. The binary tomography problem can be set in a

continuous framework, for Ω a bounded Lipschitz open subset in \mathbb{R}^2 , and $f \in L_1(\Omega)$, the Radon transform is defined by:

$$Rf(\phi, s) = \int_{\Omega \cap L(\phi, s)} f(x) dl \quad (3.1)$$

where $L(\phi, s)$ is the line determined by the polar angle $\phi \in [0, \pi)$, and the distance $s \in [-a, a]$ of the line from the origin. Recently, level-set methods have attracted much interest in the field of inverse problems to reconstruct solutions with piecewise constant solutions (Egger and Leitao, 2009; DeCezaro et al., 2009; DeCezaro et al., 2013). Yet, they have never been applied to the binary tomography reconstruction problem. For simplicity, we restrict to the binary inverse problem. We assume that the function to be reconstructed f is piecewise constant, and it can take two values 0 and 1 on disjoint measurable subsets Ω_1, Ω_2 with $\Omega = \Omega_1 \cup \Omega_2$. We assume that f is the characteristic function of a regular set:

$$f \in K = \{\chi_{\Omega_1} \text{ where } \Omega_1 \subset \Omega \text{ and } \mathcal{H}(\partial\Omega_1) < \infty\} \quad (3.2)$$

where $\mathcal{H}(\partial\Omega_1)$ is the Hausdorff measure of the boundary $\partial\Omega_1$. The function f can then be represented with the Heaviside distribution and with a level-set function $\theta \in H_1(\Omega)$ as $f = H(\theta)$, where $H_1(\Omega)$ is the first-order Sobolev space and with:

$$H(\theta) = \begin{cases} 0 & \text{if } \theta > 0 \\ 1 & \text{otherwise} \end{cases} \quad (3.3)$$

By the nonlinear transformation, the nonlinear inverse problem consists in determining the level-set function θ such that:

$$RH(\theta) = p^\delta \quad (3.4)$$

Since H is discontinuous, it is necessary to consider generalized minimizers of the regularization functional (Egger and Leitao, 2009; DeCezaro et al., 2009). These minimizers can be approximated by minimizers of smoothed regularization functional with an approximation H_ϵ . The forward operator R is continuous and Fréchet differentiable with respect to the L_1 topology (Natterer, 1986). It is possible to use the convergence results detailed in (DeCezaro et al., 2009; Egger and Leitao, 2009).

The regularization functional to be minimized is then written:

$$E(\theta) = \frac{\|RH(\theta) - p^\delta\|_2^2}{2} + F(\theta) \quad (3.5)$$

where F is a regularization term for the level-set function. In this work, we have considered a $BV - H_1$ regularization functional (DeCezaro et al., 2009; Egger and Leitao, 2009):

$$F(\theta) = \beta_1 |H(\theta)|_{BV} + \beta_2 \|\theta\|_{H_1}^2 \quad (3.6)$$

The regularization parameters β_1, β_2 determine the relative weights of the stabilizing terms. The Bounded Variation BV seminorm is given by:

$$|H(\theta)|_{BV} = \int |\nabla H(\theta)| dx \quad (3.7)$$

It penalizes the length of the Hausdorff measure of the boundary of the set Ω_1 . This contour regularization term is included in the Chan-Vese functional to prevent the zero level curves becoming oscillatory (Chan and Vese, 2001; Tai and Chan, 2004).

3.2 Implementation of the level-set regularization approach

In the numerical implementation, it is necessary to replace the Heaviside function H by smoothed approximations. These relaxations are usually used in image segmentation. The following smooth approximations of the Heaviside function H has been used:

$$H_\epsilon(x) = \frac{1 + 2\epsilon}{2} (\text{erf}(x/\epsilon) + 1) - \epsilon \quad (3.8)$$

where ϵ is a real positive constant that controls the scale of the smoothed Dirac. The smoothed Tikhonov regularization functional is given by:

$$E_\epsilon(\theta) = \frac{\|RH_\epsilon(\theta) - p^\delta\|_2^2}{2} + \beta_1 |H_\epsilon(\theta)|_{BV} + \beta_2 \|\theta\|_{H^1}^2 \quad (3.9)$$

The minimizers of the Tikhonov functionals are found with a first-order optimality condition for the smoothed functionals, $G(\theta) = 0$, with :

$$G(\theta) = H'_\epsilon R^*(RH_\epsilon(\theta) - p^\delta) + \beta_2 (I - \Delta)(\theta) + \beta_1 \frac{\partial |H_\epsilon(\theta)|_{BV}}{\partial \theta} \quad (3.10)$$

where R^* denotes the adjoint of the forward projection operator. The differential of $|H_\epsilon(\theta)|_{BV}$ is given by (Tai and Chan, 2004):

$$\frac{\partial |H_\epsilon(\theta)|_{BV}}{\partial \theta} = -\delta_D(\theta) \nabla \cdot \frac{\nabla \theta}{|\nabla \theta|} \quad (3.11)$$

where δ_D is a Dirac distribution. The solutions of the optimality condition $G(\theta) = 0$ are obtained with a Gauss-Newton method. From the current estimate θ_k , the update $\theta_{k+1} = \theta_k + \lambda \delta \theta$ is obtained with:

$$V_k^* V_k \delta \theta + \beta_2 (I - \Delta)(\delta \theta) - \beta_1 \delta(\theta_k) \nabla \cdot \frac{\nabla \delta \theta}{|\nabla \theta_k|} = -G(\theta_k) \quad (3.12)$$

where V_k is the operator $V_k = RH'_\epsilon(\theta_k)$. These symmetric linear systems are solved by a conjugate gradient method. In the above formula, λ is a relaxation parameter.

4 Piecewise constant level-set PCLS with an augmented Lagrangian approach

4.1 Piecewise constant level-set approach

In the framework of the piecewise constant level-set (PCLS) approach (DeCezaro et al., 2013), the unknown function f is represented with a smooth operator $P : L_2(\Omega) \rightarrow L_2(\Omega)$ and a piecewise constant function $\phi \in L_2(\Omega)$ as $f = P(\phi)$. In the binary tomography problem, the solution f takes the values 0 and 1, and thus it can be parametrized as $f = \phi$. In the discretized version, the assumption that the function ϕ is piecewise constant with value 0 and 1 corresponds to the constraint:

$$K(\phi) = \phi(\phi - 1) = 0 \quad (4.1)$$

where $K:L_2(\Omega) \rightarrow L_2(\Omega)$ is a smooth nonlinear operator. The binary tomography inverse problem can be formulated as:

$$R\phi = p^\delta \quad \text{where} \quad \phi \in \{L_2(\Omega) \mid K(\phi) = 0\} \quad (4.2)$$

In the augmented Lagrangian method, the former constrained optimization problem is associated with an augmented Lagrangian functional:

$$L(\phi, \lambda) = \frac{\mu \|R\phi - p^\delta\|_2^2}{2} + \beta \frac{\|K(\phi)\|_{L_2(\Omega)}^2}{2} + \int \lambda K(\phi) + |\phi|_{TV} \quad (4.3)$$

where μ is the regularization parameter, β is the Lagrange parameter, $\lambda \in L_2(\Omega)$ is a Lagrange multiplier. The solutions (f^*, λ^*) is obtained as the saddle point of the algorithm. The PCLS and LS schemes both include the binary constraints and some smoothness constraints.

4.2 Implementation of the PCLS approach

For a given penalty factor β , and starting from an initial guess (ϕ_0, λ_0) the solutions (ϕ^*, λ^*) are obtained by the optimality conditions:

$$\frac{\partial L}{\partial \phi} = 0, \quad \frac{\partial L}{\partial \lambda} = 0 \quad (4.4)$$

The level-set function and the Lagrange multiplier are updated iteratively. The updated level-set function is obtained through the minimization of the Lagrangian functional $\phi_{k+1} = \arg \min_{\phi} L(\phi, \lambda_k)$. The gradient $\frac{\partial L}{\partial \phi}$ of the Lagrangian w.r.t ϕ is given by:

$$\mu R^*(R\phi - p^\delta) + \beta K'^*(\phi)(K(\phi)) + K'^*(\phi)(\lambda) + \text{div}\left(\frac{\nabla \phi}{|\nabla \phi|}\right) \quad (4.5)$$

where $K'^*(\phi)$ is the adjoint of the Fréchet derivative of K . The iterate ϕ_{k+1} is obtained with a gradient step:

$$\phi_{k+1} = \phi_k - \frac{\partial L}{\partial \phi} \quad (4.6)$$

The Lagrange multiplier is updated with:

$$\lambda_{k+1} = \lambda_k - K(\phi) \quad (4.7)$$

5 Results and discussion

In this section, we present the simulation details and the results obtained with the Total Variation and Level-set type regularization algorithms.

5.1 Simulations details

In our experiments, the projection operator R is taken as the discrete approximation of the Radon transform, which is implemented in the Matlab Image Toolbox. The TV regularization and level-set methods were applied to two small images of size 256×256 , which are shown in Fig.1, and two large images of size 512×512 , which are shown in Fig.2. The first small image is a simple disk image and the small bone image is an experimental bone cross-sections reconstructed with 400 X-rays per projection from Filtered Back Projections (FBP) and subsequently thresholded. The large images are reconstructed with 729 projections. These images are regarded as the ground-truth images. In our simulations, these image were reconstructed from a limited number of simulated views M , with $M = 20$ and 50. For all images, the noisy projections p^δ were obtained by adding a Gaussian noise with standard deviation σ to the raw projection data p . The noise level δ can be estimated with $\delta^2 = MN_r\sigma^2$, where N_r is the number of X-rays per projection. The σ values, the $PPSNR$ values and the noise levels δ are summarized in Table.1 and Table.2.

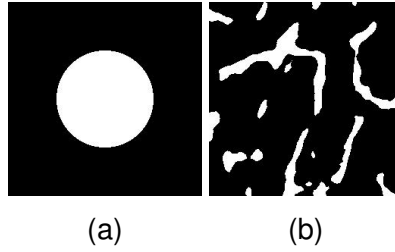


Figure 1: Small images of size 256×256 : (a) Disk image;(b) Bone cross-section image.

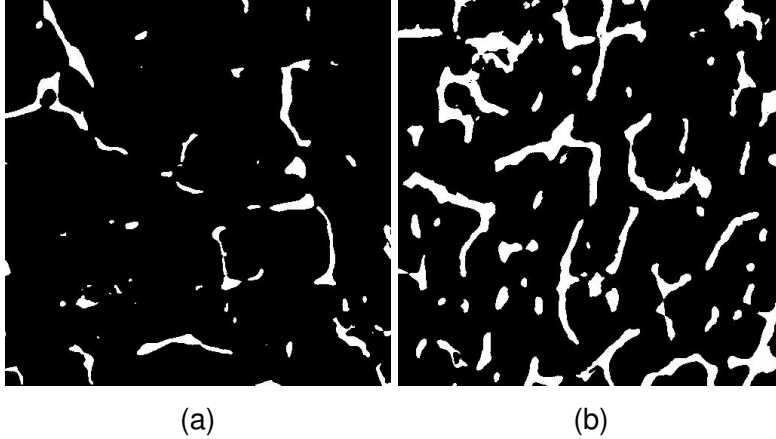


Figure 2: Large bone cross-section images of size 512×512 : (a) Sparse bone cross-section image;(b) Dense bone cross-section image.

In order to evaluate the quality of reconstruction images, the normalized error $E(k)$ and misclassification rate $MR(k)$ have been calculated as a function of the iteration number k :

$$E(k) = \frac{\|f^k - f^*\|_2}{\|f^*\|_2} \quad (5.1)$$

Table 1: Noise standards deviation σ , $PPSNR$ and δ values for small disk and bone images with 20 and 50 projections.

| σ | Small Disk image | | σ | Small bone image | |
|----------|-----------------------------------|-----------------------------------|----------|----------------------------------|-----------------------------------|
| | M=20 | M=50 | | M=20 | M=50 |
| 8.55 | $\delta = 732.4$ $PPSNR = 15$ | $\delta = 1158.1$ $PPSNR = 15$ | 6.57 | $\delta = 562.8$ $PPSNR = 14$ | $\delta = 889.4$ $PPSNR = 14$ |
| 12.83 | $\delta = 1098.6$ $PPSNR = 12$ | $\delta = 1737.2$ $PPSNR = 12$ | 9.85 | $\delta = 844.2$ $PPSNR = 11$ | $\delta = 1334.1$ $PPSNR = 11$ |
| 25.65 | $\delta = 2197.3$ $PPSNR = 7$ | $\delta = 3474.4$ $PPSNR = 7$ | 19.71 | $\delta = 1688.4$ $PPSNR = 6$ | $\delta = 2668.3$ $PPSNR = 6$ |

Table 2: Noise standard deviation σ , $PPSNR$ and δ values for big sparse and dense images with 20 projections.

| σ | Big images | |
|----------|-----------------------------------|-----------------------------------|
| | Sparse | Dense |
| 3 | $\delta = 365.6$ $PPSNR = 19$ | $\delta = 368.02$ $PPSNR = 25$ |
| 6 | $\delta = 731.16$ $PPSNR = 14$ | $\delta = 736.16$ $PPSNR = 19$ |

where f^k is the grey-level reconstructed image at the iteration k , and f^* is the ground-truth image and

$$MR(k) = \frac{N_d^k}{N} \times 100\% \quad (5.2)$$

where N_d^k is the number of different pixels between the reconstructed binary image f_b^k and the ground-truth, and N the total number of pixels. The binary image is obtained with 0.5 as the threshold.

The iterations are stopped when the regularization functional stagnates. At the end of the optimization process, E_m will denote the minimum error for grey-level images f^m obtained at the final iteration m and MR_m the minimum misclassification rate. The final iteration index m is determined by the stopping condition $\|f^{m+1} - f^m\|_2 / \|f^m\|_2 < 0.0001$.

In order to obtain the best reconstruction results, it is necessary to choose optimal regularization parameters. We have made an extensive sweeping of the values of the regularization parameters. Our choice of the optimal ones is based on the Morozov discrepancy principle (Morozov, 1984). In most cases, the parameters which are chosen such as the final iterate, f^m , satisfies the condition:

$$\|Rf^m - p^\delta\| \approx \delta \quad (5.3)$$

where δ is the noise level. For the TV regularization method, there are two important parameters: the regularization parameter μ and Lagrangian parameter β . The β parameter controls the speed of convergence. The reconstructed image $f^m(\mu)$ obtained at the end of the opti-

mization process depends only on the regularization parameter μ . In order to find the best combination of these parameters, we have tested many values of β and μ . In our numerical simulations, the regulation parameter μ and the Lagrange parameter β are selected when they satisfy the condition: $\frac{\|Rf^m - p^\delta\|}{\delta} \leq \xi$, with $\xi = 0.01$. In the classical level-set algorithm, the real positive constant ϵ which controls the smoothed Heaviside function was set to 0.03. The regularization parameter β_1 was set to 0 because the H_1 term dominates the BV term (DeCezaro et al., 2009; Egger and Leitao, 2009). Similarly to the methodology used for the TV regularization, we tested many parameters for the level-set algorithms to satisfy the Morozov principle. When the minimum of the data term is well-above the noise level, the Morozov principle can not be applied, but a good estimate of the optimal regularization parameters was obtained with the L-curve method (Hansen, 2001). Finally, the difference map image f_{diff} is used to evaluate the quality of binary images by visual inspection. It is defined as the difference between binary image f_b^m at the end of the iterative algorithms and the ground-truth image f^* :

$$f_{diff} = |f_b^m - f^*| \quad (5.4)$$

5.2 Numerical results

5.2.1 Small images

The small disk reconstruction images and the small bone cross-section reconstruction images obtained for $\sigma = 12.83$ and $\sigma = 9.85$ with the various regularization methods are displayed in Fig.3 and Fig.4 respectively. The upper images are the binary reconstruction images and the difference maps are in the lower part. The reconstruction images are localized on the boundaries.

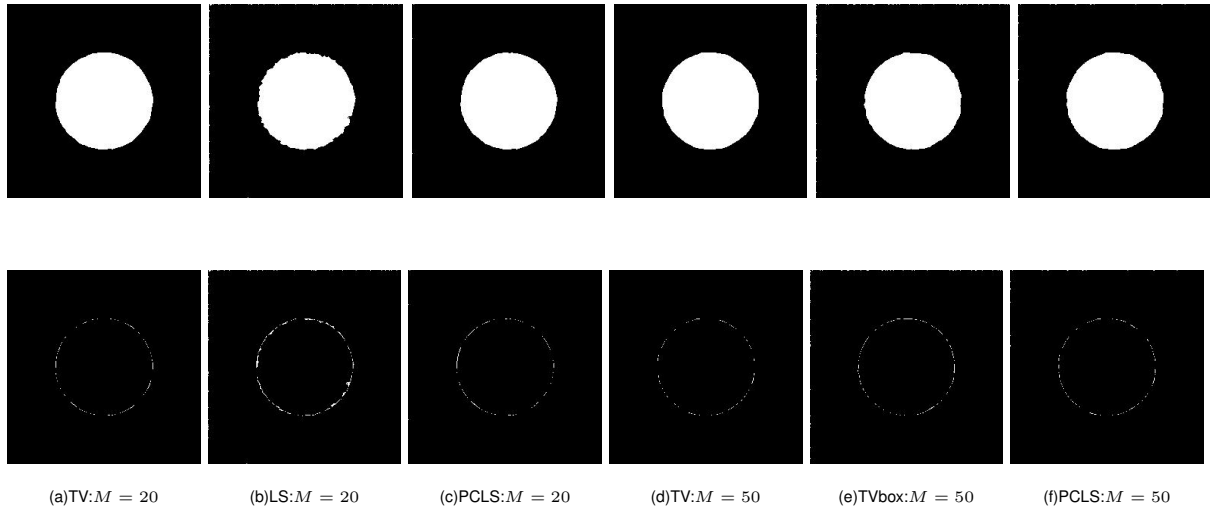


Figure 3: Disk reconstruction images with $\sigma = 12.83$, 20 and 50 projection angles, 367 X-rays per projection. The binary reconstruction images are displayed in the upper part of the figure and the difference maps are in the lower part.

The evolution curves of data term ($\|Rf^k - p^\delta\|$), normalized error ($E(k)$) and misclassification rate ($MR(k)$) with the iteration number are shown in Fig.5 and Fig.6 for the small bone image

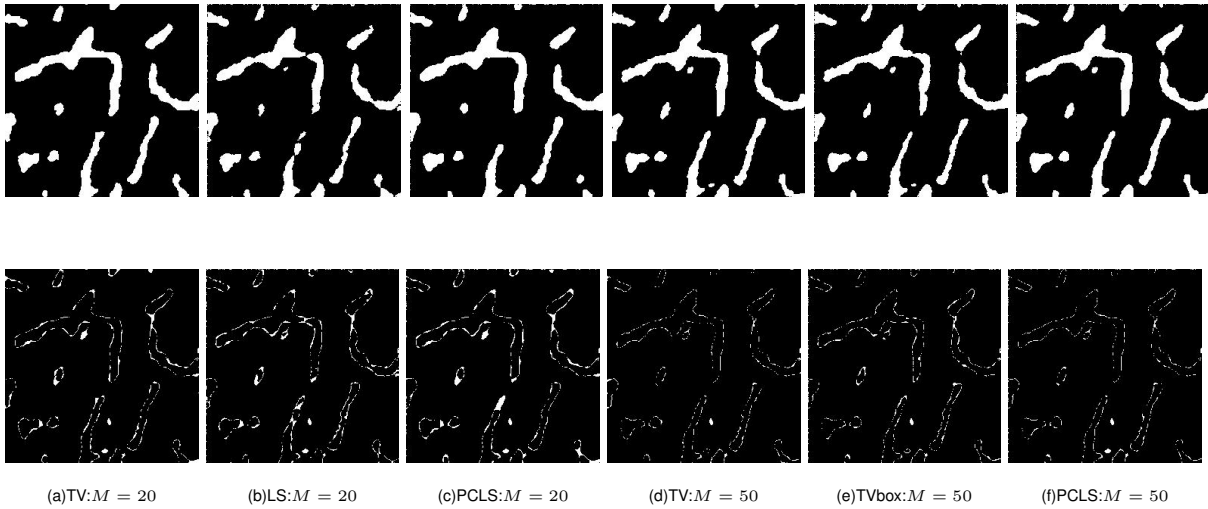


Figure 4: Bone reconstruction images with $\sigma = 9.85$, 20 and 50 projection angles, 367 X-rays per projection. The binary reconstruction images are displayed in the upper part of the figure and the difference maps are in the lower part.

with $\sigma = 9.85$, 20 and 50 projection angles.

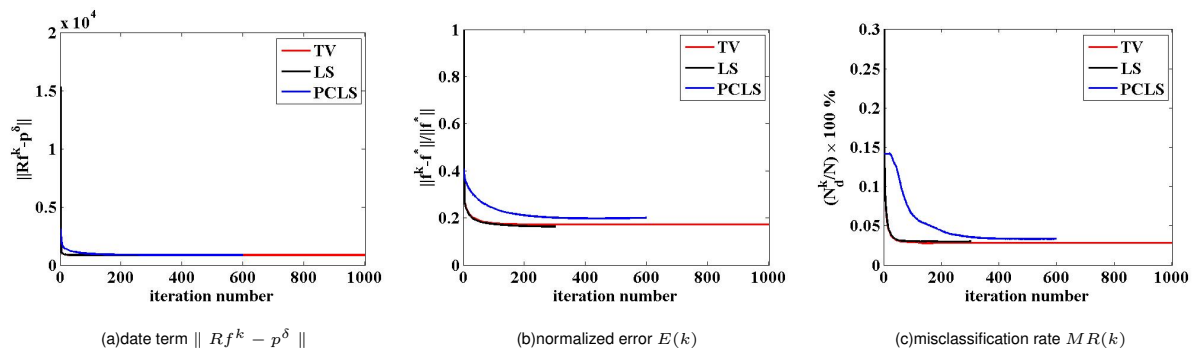


Figure 5: Evolution curves of the data term, of the normalized error and of the misclassification rate with the iteration number for small bone image with $\sigma = 9.85$, 20 projection angles.

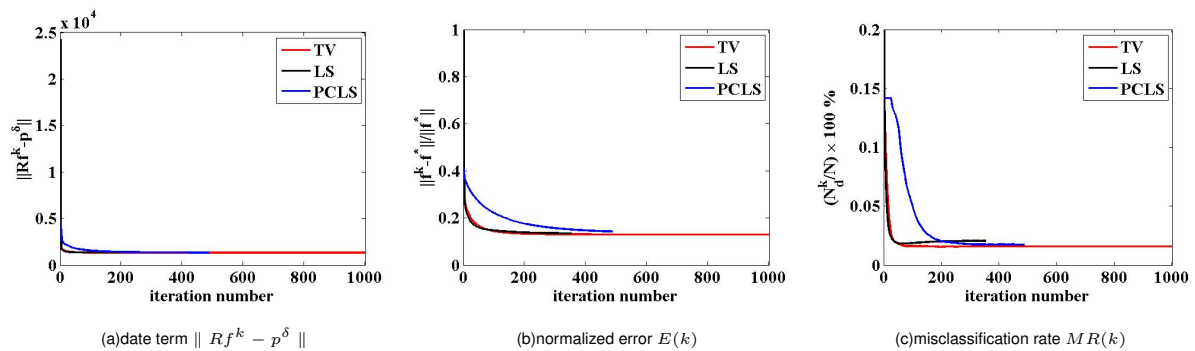


Figure 6: Evolution curves of the data term, of the normalized error and of the misclassification rate with the iteration number for small bone image with $\sigma = 9.85$, 50 projection angles.

Table.3, Table.4 summarize the minimum error E_m for each image and noise level with 20 and 50 projections, together with the minimum misclassification rate MR_m obtained, by using TV regularization, level-set regularization and PCLS method respectively.

Table 3: Minimum errors E_m and misclassification rate MR_m for small disk image with 20 and 50 projections.

| σ | TV | | LS | | PCLS | |
|----------|-----------------------------------|------------------------------------|-----------------------------------|-----------------------------------|-----------------------------------|-----------------------------------|
| | M=20 | M=50 | M=20 | M=50 | M=20 | M=50 |
| 8.55 | $E_m = 0.0505$ $MR_m = 0.15\%$ | $E_m = 0.0436$ $MR_m = 0.093\%$ | $E_m = 0.0603$ $MR_m = 0.29\%$ | $E_m = 0.0525$ $MR_m = 0.2\%$ | $E_m = 0.1060$ $MR_m = 0.19\%$ | $E_m = 0.0463$ $MR_m = 0.11\%$ |
| 12.83 | $E_m = 0.0535$ $MR_m = 0.18\%$ | $E_m = 0.0481$ $MR_m = 0.14\%$ | $E_m = 0.0702$ $MR_m = 0.43\%$ | $E_m = 0.0612$ $MR_m = 0.31\%$ | $E_m = 0.1134$ $MR_m = 0.2\%$ | $E_m = 0.0664$ $MR_m = 0.22\%$ |
| 25.65 | $E_m = 0.0737$ $MR_m = 0.42\%$ | $E_m = 0.0563$ $MR_m = 0.27\%$ | $E_m = 0.1198$ $MR_m = 1.13\%$ | $E_m = 0.0862$ $MR_m = 0.66\%$ | $E_m = 0.1626$ $MR_m = 0.79\%$ | $E_m = 0.1103$ $MR_m = 0.57\%$ |

Table 4: Minimum errors E_m and misclassification rate MR_m for small bone image with 20 and 50 projections.

| σ | TV | | LS | | PCLS | |
|----------|-------------------------------------|-------------------------------------|-------------------------------------|-------------------------------------|-------------------------------------|-------------------------------------|
| | M=20 | M=50 | M=20 | M=50 | M=20 | M=50 |
| 6.57 | $E_m = 0.1476$, $MR_m = 2.11\%$ | $E_m = 0.1041$, $MR_m = 1.01\%$ | $E_m = 0.1442$, $MR_m = 2.32\%$ | $E_m = 0.1192$, $MR_m = 1.68\%$ | $E_m = 0.2088$, $MR_m = 3.44\%$ | $E_m = 0.1324$, $MR_m = 1.11\%$ |
| 9.85 | $E_m = 0.1714$ $MR_m = 2.82\%$ | $E_m = 0.1292$ $MR_m = 1.58\%$ | $E_m = 0.1634$ $MR_m = 2.99\%$ | $E_m = 0.1346$ $MR_m = 2.05\%$ | $E_m = 0.1976$ $MR_m = 3.33\%$ | $E_m = 0.1370$ $MR_m = 1.69\%$ |
| 19.71 | $E_m = 0.2128$ $MR_m = 4.9\%$ | $E_m = 0.0258$ $MR_m = 2.58\%$ | $E_m = 0.2046$ $MR_m = 4.63\%$ | $E_m = 0.1657$ $MR_m = 3.05\%$ | $E_m = 0.2446$ $MR_m = 6.23\%$ | $E_m = 0.1814$ $MR_m = 2.80\%$ |

From these tables, we can infer that for small images, the TV regularization algorithm gives in most cases the best reconstruction results with 20 and 50 projections. For the simple disk image, PCLS method works better than LS algorithm. While for the small bone image, the LS method works better than PCLS algorithm for few projection. For a low number of projections (M=20) and a high noise level, the LS approach may outperform the TV regularization. When the problem is very ill-posed and for complex structure the TV term which favors disk like structures is not the most efficient a priori.

5.2.2 Large bone cross-section images

The three algorithms were also compared on bone cross-sections images of size 512×512 , and two noise levels $\sigma = 3$, $\sigma = 6$ have been tested. The evolution of normalized errors of grey-level images with iteration number are very similar to the ones obtained with the small images.

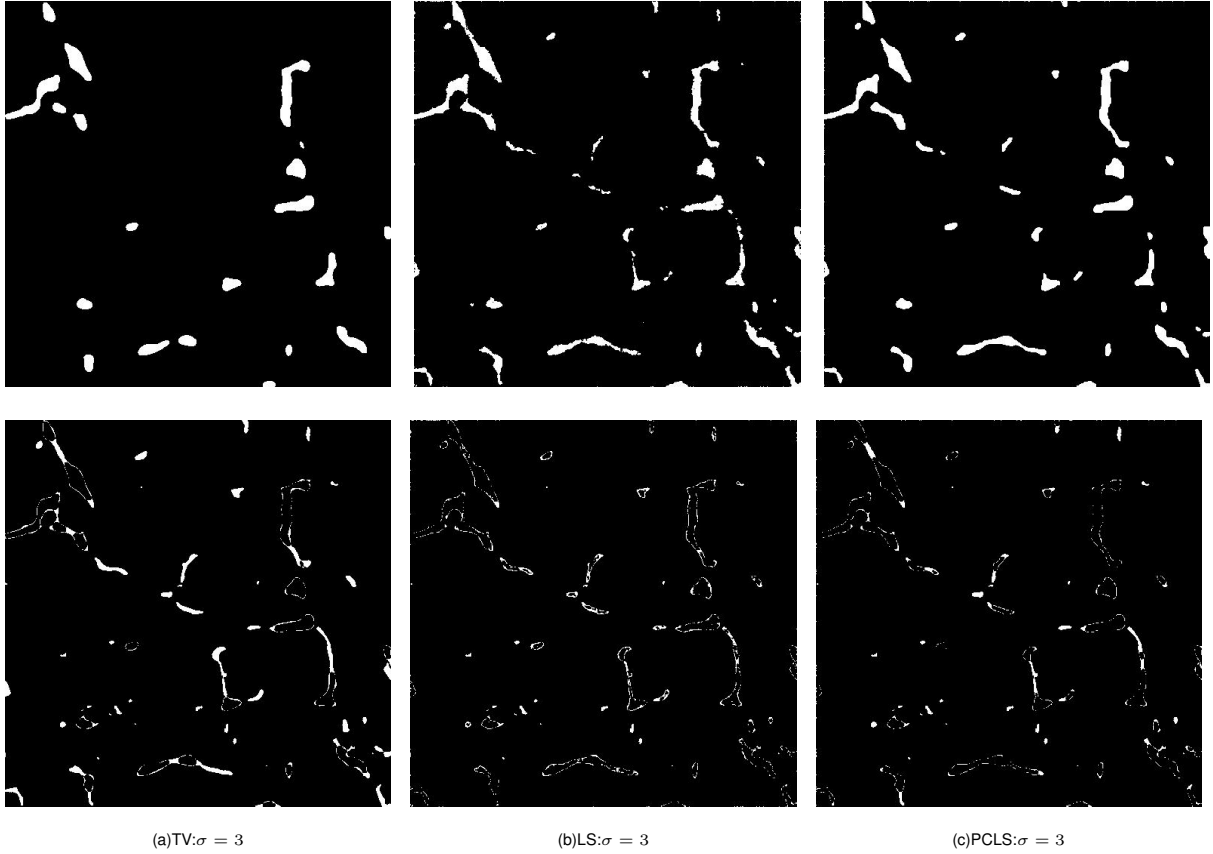


Figure 7: Sparse bone reconstruction images with $\sigma = 3$, 20 projection angles and 729 X-rays per projection. The binary reconstructed images are displayed in the upper part of the figure and the difference maps are in the lower part.

The evolution curves of data term ($\|Rf^k - p^\delta\|$), normalized error ($E(k)$) and misclassification rate ($MR(k)$) with the iteration number are shown in Fig.9 and Fig.10 for the big sparse bone image with $\sigma = 3$ and $\sigma = 6$, and 20 projection angles. The evolution curves for the big dense bone image are very similar. The binary reconstruction obtained for sparse images are shown in Fig.7, Fig.8 for TV regularization algorithm, level-set method (LS) and (PCLS) method.

Table.5 summarizes the minimum error E_m and minimum misclassification rate MR_m obtained for low density and high density bone cross-section images with 20 projections. From this table, it is obvious that TV regularization method is the worst reconstruction method for large images. It is impossible to find a regularization parameter μ and a Lagrange parameter β to make the data term $\frac{\|Rf^m - p^\delta\| - \delta}{\delta} \leq \xi$, with $\xi = 0.01$ for TV algorithm. In our simulations, the smallest constant ξ which satisfies this relation is $\xi = 0.5$. The PCLS method is better than LS algorithm when the noise level is low. The TV method performs poorly on large bone cross-sections with complex and elongated regions. Some details and fine structures are lost with the TV a priori which minimize the perimeters of the boundaries. The level-set regularization includes some constraint that favor the binary values and improves reconstruction results.

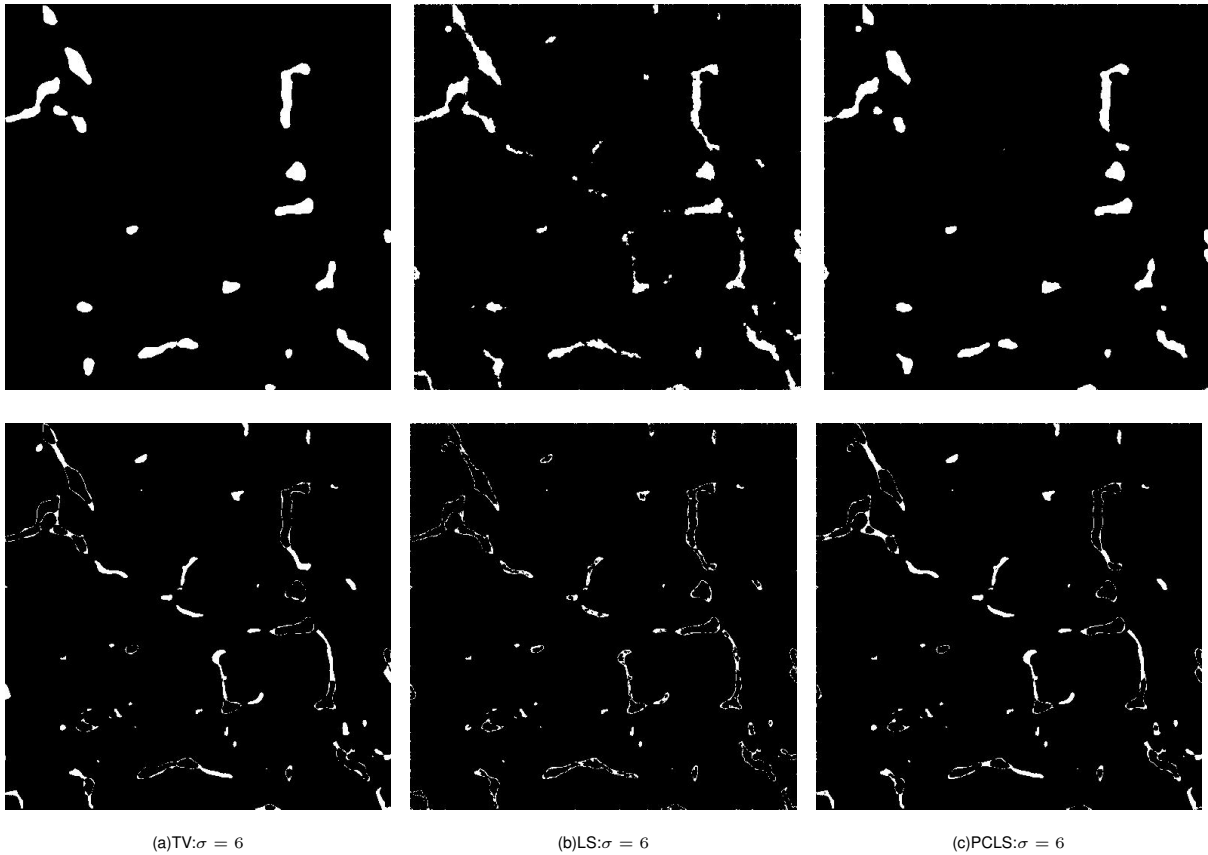


Figure 8: Sparse bone reconstruction images with $\sigma = 6$, 20 projection angles and 729 X-rays per projection. The binary reconstructed images are displayed in the upper part of the figure and the difference maps are in the lower part.

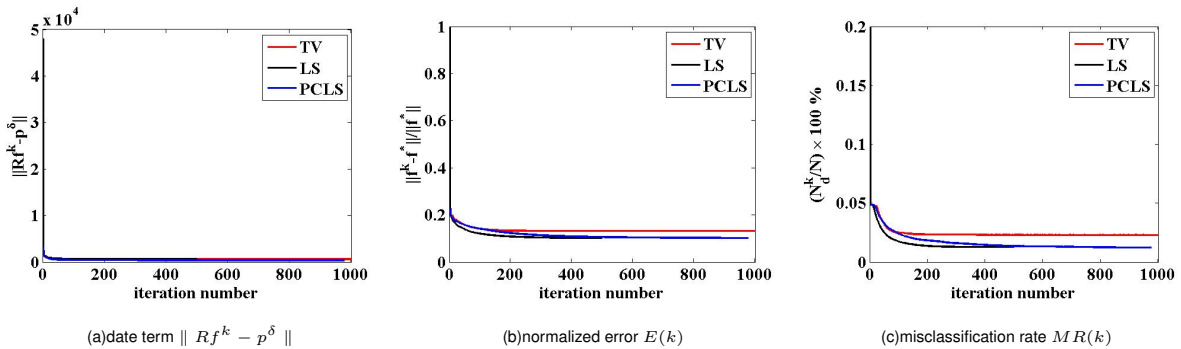


Figure 9: Evolution curves of data term, normalized error and misclassification rate with the iteration number for big sparse bone image with $\sigma = 3$, 20 projection angles.

6 Conclusion

In this paper, three reconstruction methods for binary tomography with a limited number of projections have been compared. Two new algorithms have been studied in detail. The first method is the classical TV based regularization approach. The optimal solution is obtained with the ADMM algorithm. The two others approaches are level-set regularizations never ap-

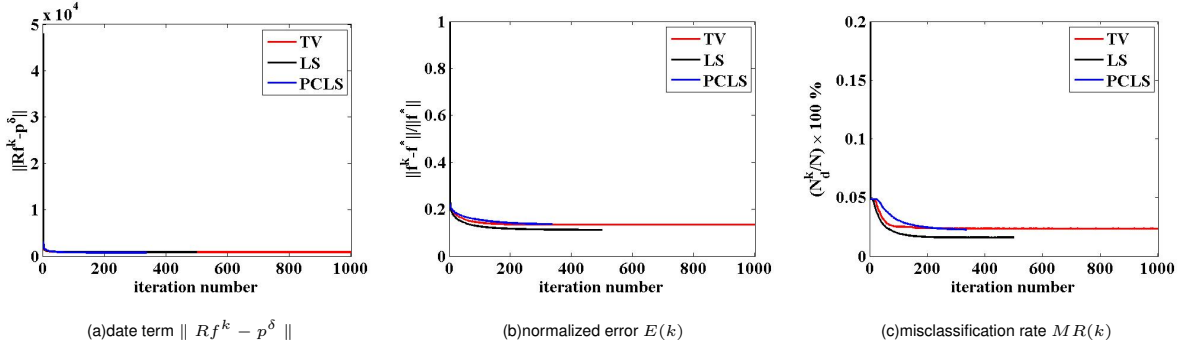


Figure 10: Evolution curves of data term, normalized error and misclassification rate with the iteration number for big sparse bone image with $\sigma = 6$, 20 projection angles.

Table 5: Minimum errors E_m and misclassification rate MR_m for small bone image with 20 and 50 projections.

| σ | TV | | LS | | PCLS | |
|----------|-----------------------------------|-----------------------------------|-----------------------------------|-----------------------------------|-----------------------------------|-----------------------------------|
| | Sparse | Dense | Sparse | Dense | Sparse | Dense |
| 3 | $E_m = 0.1320$ $MR_m = 2.33\%$ | $E_m = 0.2299$ $MR_m = 5.61\%$ | $E_m = 0.1015$ $MR_m = 1.27\%$ | $E_m = 0.1739$ $MR_m = 3.09\%$ | $E_m = 0.1016$ $MR_m = 1.22\%$ | $E_m = 0.1580$ $MR_m = 2.71\%$ |
| 6 | $E_m = 0.1342$ $MR_m = 2.35\%$ | $E_m = 0.2332$ $MR_m = 5.59\%$ | $E_m = 0.1117$ $MR_m = 1.6\%$ | $E_m = 0.1854$ $MR_m = 3.81\%$ | $E_m = 0.1365$ $MR_m = 2.26\%$ | $E_m = 0.2202$ $MR_m = 4.85\%$ |

plied to the binary tomography problem. The first level-set method is based on a representation of the function to be reconstructed with a Heaviside distribution which leads to a nonlinear inverse problem formulation of the binary tomography problem. The second one (PCLS) uses piecewise constant functions and a minimization of an augmented Lagrangian including the binary constraint. The performance of these algorithms are compared under different levels of Gaussian noise on two small images (a disk image and CT bone cross-section image) and two large images (sparse and dense CT bone cross-section images) with different number of projections. The regularization parameters are carefully chosen with the Morozov discrepancy principle. For the small images, the minimum reconstruction errors are obtained with the TV scheme both for disk and bone images, except for a low number of projections and a high level of noise. For the large images, the best minimum errors and misclassification rates were obtained by PCLS algorithm when $\sigma = 3$, with LS method when $\sigma = 6$. The level-set approaches include some constraint favoring the binary values and outperforms the TV scheme for the complex bone cross-sections. In future work, the same comparison will be applied to real images. The method will be extended to 3D images. Some stochastic methods will be investigated to decrease the reconstruction errors on the boundaries.

References

- Afonso, M., Bioucas-Dias, J. and Figueiredo, M. 2010. Fast image recovery using variable splitting and constrained optimization, *IEEE Transactions on Image Processing* **19**(9): 2345–2356.
- Afonso, M., Bioucas-Dias, J. and Figueiredo, M. 2011. An augmented Lagrangian approach to the constrained optimization formulation of imaging inverse problems, *SIAM Journal on Scientific computing* **20**(3): 681–695.
- Batenburg, K. J. and Sijbers, J. 2009. Generic iterative subset algorithm for discrete tomography, *Discrete Applied Mathematics* **157**: 438–451.
- Becker, S., Bobin, J. and Candes, E. 2009. NESTA: A fast and accurate first-order method for sparse recovery, *SIAM Journal on Scientific computing* **4**: 1–39.
- Cai, W. and Ma, L. 2010. Comparaison of approaches based on optimization and algebraic iteration for binary tomography, *Computer Physics Communications* **181**: 1974–1981.
- Capricelli, T. and Combettes, P. 2007. *Advances in discrete tomography and its applications: A convex programming algorithm for noisy discrete tomography*, Birkhauser, Boston, MA.
- Chan, T. and Vese, L. 2001. Active contours without edges, *IEEE Transactions on Image Processing* **10**: 266–277.
- DeCezaro, A., Leitao, A. and Tai, X. C. 2009. On multiple level-set regularization methods for inverse problems, *Inverse Problems* **25**(035004).
- DeCezaro, A., Leitao, A. and Tai, X. C. 2013. On piecewise constant level-set (PCLS) methods for the identification of discontinuous parameters in ill-posed problems, *Inverse Problems* **29**(015003).
- Egger, A. and Leitao, L. 2009. Nonlinear regularization for ill-posed problems with piecewise constant or strongly varying solutions, *Inverse Problems* **25**(115014).
- Gouillart, E., Krzakala, F., Mezard, M. and Zdeborov, L. 2013. Belief propagation reconstruction for discrete tomography, *Inverse Problems* **29**(035003).
- Hansen, P. C. 2001. *The L-curve and its use in the numerical treatment of inverse Pproblems*, Advances in Computational Bioengineering, WIT Press, Southampton.
- Herman, G. T. and Kuba, A. 2007. *Advances in discrete tomography and its applications*, Applied and Numerical Harmonic Analysis, Birkhauser, Boston, MA.
- Liao, H. Y. and Herman, G. 2004. Automated estimation of the parameters of the Gibbs priors to be uses in binary tomography, *Discrete Applied Mathematics* pp. 249–170.
- Morozov, V. A. 1984. *Methods for solving incorrectly posed problems*, Springer-Verlag, Berlin-Heidelberg-New York-Toky.

- Natterer, F. 1986. *The mathematics of computerized tomography*, Wiley-Teubner series in computer science, Vieweg+Teubner Verlag, UK.
- Ng, M. K., Weiss, P. and Yuan, X. 2010. Solving constrained total-variation image restoration and reconstruction problems via alternating direction methods, *SIAM Journal on Scientific computing* **32**: 2710–2736.
- Ritschl, L., Bergner, F., Fleischmann, C. and Kachelriess, M. 2011. Improved total variation-based CT image reconstruction applied to clinical data, *Phys.Med.Biol.* **56**: 1545–1561.
- Rudin, L. I., Osher, S. and Fatemi, E. 2013. Nonlinear total variation based noise removal algorithms, *Phys.D.* **60**: 259–268.
- Rusko, L. and Kuba, A. 2005. Multi-resolution methods for binary tomography, *Electronics Notes in Discrete Mathematics* **20**: 299–311.
- Schlea, T., Schnrra, C., Webera, S. and Horneggerb, J. 2005. Discrete tomography by convex-concave regularization and D.C programming, *Discrete Applied Mathematics* **151**: 229–243.
- Sidky, E. Y. and Pan, X. 2006. Accurate image reconstruction from few-views and limited-angle data in divergent-beam CT, *J.X-ray Sci. Techn.* **14**: 119–139.
- Sidky, E. Y. and Pan, X. 2008. Image reconstruction in circular cone-beam computed tomography by constrained total variation minimization, *Phys.Med.Biol.* **53**: 4777–4807.
- Tai, X. C. and Chan, T. 2004. A survey on multiple level-set methods with applications for identifying piecewise constant functions, *International Journal of Numerical Analysis and Modeling* **1**: 25–47.